Geostatistical modelling of the spatial life history of post-larval deep-water hake (*Merluccius paradoxus*) in the Benguela Current Large Marine Ecosystem

Teunis Jansen[1,5] and Uffe Høgsbro Thygesen[5]

The following scientists contributed to the study but time constraints has not permitted them to comment the final version of this working document: Kasper Kristensen[5], Paulus Kainge[2], Deon Durholtz[3], Tore Strømme[4], John Kathena[2], Tracey P. Fairweather[3], Jan E. Beyer[5]

1) BCC – Benguela Current Commission, Private Bag 5031, Swakopmund, Namibia.
2) MFMR – Ministry of Fisheries and Marine Resources, PO Box 912, Swakopmund, Namibia.
3) DAFF – Department for Agriculture, Forestry & Fisheries, Cape Town, South Africa.
4) Institute of Marine Research, P.O. Box 1870 Nordnes, N-5817 Bergen, Norway.
5) DTU AQUA – National Institute of Aquatic Resources, Charlottenlund, Denmark

Keywords: *Hake, Benguela Current, Merluccius paradoxus, migration, population structure, trans-boundary, natal homing, geostatistics, LGC, TMB, Template Model Builder, South Africa, Namibia, demersal trawl, mortality*

Corresponding author: Teunis Jansen; DTU AQUA - *National Institute of Aquatic Resources, Technical University of Denmark; Charlottenlund castle, 2920 Charlottenlund, Denmark; Tel.: +4530667840; Fax: +4533963333; E-mail address:* Tej@aqua.dtu.dk.

1. Introduction

Deep-water hake (*Merluccius capensis*) is among the dominant demersal fish species in the Benguela Current Large Marine Ecosystem (BCLME), a productive upwelling system off the west coast of Southern Africa (5-37ºS, 0-26ºE). *M. paradoxus* inhabit the continental shelf slope from around 17ºS in Angola/Namibia to about 27ºE in South Africa (Figure 1) (Payne, 1995).

M. paradoxus spawn mainly in areas of 200–650 m bottom depths between 34.5◦S and 36.5◦S on the South African west coast. Spawning individuals has been found as far as 25ºS in Namibia and 27ºE off the South African south coast at depths ranging from 170 to 837 m (Jansen et al., 2015a). Spawning off the South African coast takes place throughout the year, with increased intensity around March and August–October (Jansen et al., 2015a).

Onshore, Offshore and alongshore ontogenetic migration has been indicated for *M. paradoxus* (Le Clus et al., 2005; Strømme et al., 2016). Based on catch rates by length class from South African surveys between 1990 and 2003, Le Clus et al (2005) concluded that *M. paradoxus* on the west and south coast was connected and likely belonged to the same stock. Strømme et al. (2016) extended this view to include Namibia where they found a large proportion of late juveniles, indicating a southern origin and a subsequent spawning migration to back to South Africa as the hakes matured. Juveniles initially migrate to shallower waters followed by a lifelong movement towards deeper waters (Botha, 1980; Burmeister, 2001; Gordoa and Duarte, 1991; Payne and Punt, 1995; Strømme et al., 2016). Large *M. paradoxus* has been found down to 1000 m (Burmeister, 2001; Mas-Riera, 1991).

The spatio-temporal spawning and migration patterns are in accordance with the most recent and comprehensive genetic study of *M. paradoxus* that found no spatial divergence and concluded in accordance with (Bloomer et al., 2009) that the population structure is one panmictic stock (Henriques et al., 2016). The authors found significant temporal divergence and suggested that this was from genetic chaotic patchiness. An earlier study had pointed towards multiple stocks (von der Heyden et al., 2010).

The area around the Lüderitz upwelling cell and Orange River Cone (LUCORC) region (25º-29ºS) forms a natural barrier between the northern Benguela and southern Benguela (Agenbag

and Shannon, 1988; Lett et al., 2007; Rae, 2005). Therefore, and for practical/political simplicity, the national border between Namibia and South Africa (Orange River at 29 °S) is still regarded as the boundary dividing the *M. paradoxus* into two management stocks (Figure 1) (Burmeister, 2005; Grant et al., 1988, 1987). The stock assessment and fisheries management advice has not yet adopted to the new understanding of *M. paradoxus* as one panmictic stock that migrate across the border between Namibia and South Africa. It is therefore unknown if the current fisheries practice for *M. paradoxus* in the BCLME is sustainable and optimal.

Recent developments in geostatistics and model fitting has facilitated analyses of large datasets from trawl surveys and let to new biological insight (Jansen et al., 2016, 2014; Kristensen et al., 2014).

In the present study we apply these methods to a large dataset of survey data from Namibia and South Africa to exhibit the spatial life history of post-larval *M. paradoxus*. This is the first analysis of *M. paradoxus* integrated both the South African, Namibian and Norwegian surveys.

We aim to test if the data supports the hypothesis of one panmictic stock and transboundary migration. Furthermore, we quantify the size specific migration for future usage in improved stock assessments.

2 Materials and methods

The data used for this study were the same as used by Jansen et al. (2016), except that data from 2012 were not available for *M. paradoxus*. Modelling, post-processing and presentation of the results also followed the methods and design described in Jansen et al. (2016). The following description of materials and methods is therefore a modified copy from Jansen et al. (2016).

2.1 Scientific trawl survey data

The dataset used in this study comprised data from demersal trawl surveys conducted during the period 1998–2011 in the Benguela-Agulhas ecosystem between 17°S (northern border of Namibia) and 27°E on the South African south coast (Figure 1). All surveys sampled the demersal fish community on the continental shelf and upper shelf slope.

Namibian surveys used a Gisund Super demersal trawl towed by chartered commercial trawlers, all inter-calibrated with the *R/V Dr Fridtjof Nansen*, and the data were made available by the Ministry of Fisheries and Marine Resources (MFMR) in Namibia. Namibia surveys followed a systematic transect design with resampling of fixed transects with a semi-random distribution of stations along the transects. The South African surveys were conducted using either the "old" or the "new" configuration of a German 4-panel bottom trawl onboard *R/V Africana*. A few surveys were also conducted in South African waters using the Gisund trawl onboard *R/V Dr. Fridtjof Nansen*. South Africa surveys followed a random stratified sampling survey design. Details on the three types of gear, their operation and rigging are available in Axelsen and Johnsen (2015). Trawling time was approximately 30 minutes, and data from hauls shorter than 25 mins or longer than 35 were excluded from the analysis. Data from *R/V Africana* were made available by the Department of Agriculture Forestry and Fisheries (DAFF) in South Africa and data from *R/V Dr. Fr. Nansen* were provided by FAO/Norway (IMR). No trawl samples were available from Angolan waters due to species identification problems between *M. capensis*, *M. paradoxus* and *M. polli* (Benguela hake, which is largely caught in Angola).

For each trawl haul, the total catch was weighed and sorted to species level where possible. Large catches were subsampled. The weight of all *M. capensis* in the catch was recorded and total lengths of a subset of the individuals were measured in cm (rounded down). The length data recorded from the subsamples were subsequently raised to estimate the length composition in the total catch.

Data collected from nine hauls where winds in excess of 25 knots may have compromised the performance of the gear and hence the associated data points (Wieland et al., 2013) were excluded from the dataset.

The final survey dataset comprised 6 343 trawl hauls from 1998 to 2011, 57 % of which contained *M. paradoxus*. Catches (in numbers) ranged from 0 to 29 844 *M. paradoxus* per haul, with a mean catch of 867 in the non-zero hauls. The data set comprised a total of 3.1 million records of *M. paradoxus* lengths. Samples were available from the entire region except the shallow area (20 - 100 m) in central Namibia that is characterized by untrawlable bottom (Figure 1). The samples were relatively equally distributed over the time-series (Fig. 2a). Most samples in Namibia and on the South African west coast were taken in January-February, while the South

116 African south coast was generally sampled in April-May (Figure 2b). Trawling was
117 predominately done during the day (Figure 2c) at depths from 20 to 960 m (Figure 2d). The catch
118 numbers from gears other than Gisund (i.e. "old" Africana and "new" Africana) were
119 deterministically converted to the Gisund equivalent catch using the estimated length-specific
120 gear effect from supplementary information 1.

121 The difference in the timing of the surveys in the various sub-regions in addition to the
122 spawning phenology made it impossible to estimate the exact age of the hakes. M. paradoxus
123 spawn throughout the year with increased intensity around March and August–October (Jansen
124 et al., 2015a). The northern parts of the region (central Namibia) were surveyed in January to
125 February (mean = 30 January). Consequently, the recruits in Namibia were primarily surveyed
126 approximately 4.5 and 10.5 months after spawning. The South African west coast was also
127 surveyed in January to February. Off the South African south coast surveys took place three
128 months later (April-May, mean = 26 April). The young-of-the-year hake therefore entered the
129 survey catches at various sizes and ages. For illustration purposes, mean age of the young-of-the-
130 year hakes that entered the catches were set to 6 months.

131 *2.2 The GeoPop model*

132 Log Gaussian Cox (LGC) process modelling with correlations was used to describe
133 abundance indices of *M. paradoxus* cohorts through space and time and along environmental
134 gradients, observed using various gear types, as the hake recruited, grew and died. Similar
135 models have previously proved their value for mackerel larvae and juveniles (Jansen et al.,
136 2015b, 2012), cod (*Gadus morhua*) (Kristensen et al., 2013; Lewy and Kristensen, 2009),
137 whiting (*Merlangius merlangus*) (Nielsen et al., 2014), and shallow-water hake (*Merluccius*
138 *capensis*) (Jansen et al., 2016).

139 The first attempts to fit this type of model to the hake data from demersal surveys were
140 unsuccessful because the large number of latent variables that needed to be estimated in this 4D-
141 problem exceeded the limits of the physical processing power. The recent advent of the Template
142 Model Builder (TMB; Kristensen et al., 2015) – a software library that can fit random effect
143 models much faster than AD model Builder (Fournier et al., 2012) provided a solution to this
144 obstacle. Physical processing power was furthermore increased by running the software on an
145 r3.8xlarge instance under Amazon Elastic Compute Cloud (Amazon EC2). TMB was installed

on Linux on the r3.8xlarge platform consisting of 32 CPUs (2.5 GHz Intel Xeon E5-2670 v2, AVX and turbo boost), 244 GiB RAM and 2 x 320 GB SSD storage (https://aws.amazon.com/ec2/instance-types/). This setup facilitated the study of *M. capensis* in a rich dataset by a complex model – a study that was impossible with ADMB or the model fitting algorithms provided in the LGC-package used by Kristensen et al. (2013). The same setup was used in the present study of *M. paradoxus.*

The model formulation and notation used for this study was identical to that described by Kristensen et al. (2013). The response variable was catch in numbers from 47 size classes (2 cm bins from 5 to 99 cm) in annual time steps in the period 1998 to 2011. The model consisted of four main elements: The large scale spatio-temporal aspects ($\eta(s,x,t)$), the local patchiness ($\eta_0(s,j)$, the population dynamics size-spectrum ($\phi(s,t)$) and the gear selectivity ($sel(s)$). In the log-domain, the sum of these four components equals the total (latent) log intensity of the poisson measurements indexed by haul-id *j*:

$$\log(\lambda(s_j,x_j,t_j)) = \eta(s_j,x_j,t_j) + \eta_0(s_j,j) + \phi(s_j,t_j) + \log(sel(s_j))$$ For the first three elements the variance parameters are denoted by σ^2, σ_N^2 and σ_ε^2, respectively. Conditional on the intensity λ, the counts (i.e. the number of *M. paradoxus* in each size class in a haul taken at a particular point in space and time, with a particular gear) were assumed to be Poisson distributed (Kristensen et al., 2013). This implied a resulting (unconditional) distribution with much higher dispersion than the Poisson. This model structure is referred to as a log Gaussian Cox process model and has been shown to be appropriate for count data from catches that are over-dispersed and zero-inflated (with many zero values) (Jansen et al., 2015b; Kristensen et al., 2013). The Poisson distribution allows for zero catches, while the log Gaussian randomness imply over-dispersed catches (relative to Poisson), both allowing for very high counts and for many more zero catches than would be found in a pure Poisson model.

The large scale spatio-temporal element ($\eta(s,x,t)$) was a key feature of the model. It models the time-varying heterogeneous spatial distribution of a size-structured population. The statistical properties of this distribution were modelled in three parts: large-scale spatial patterns (correlations between cells), temporal fluctuations (correlations between years) and size structure (correlations between catches in different size classes). All correlations were assumed to decay exponentially with spatial distance, time lag, and size difference, respectively, and assumed to be

multiplicative. The spatial correlation was assumed to be isotropic (direction independent). In order to avoid correlation over land (e.g. the Cape region in South Africa), the spatial correlation effect was modelled as a Gaussian Markov random field (cell-to-cell chains). The parameter estimates for these correlations were expressed as decorrelation distance (*H*), decorrelation time (*T*) and decorrelation size (*L*), which were the distances in space, time or size where the correlations had decayed to e^{-1} (explaining ca. 14% of the variance). Documentation of these correlation structures were published in Kristensen *et al.* (2013). The spatio-temporal fields were represented by annual time steps covering the 14 years of the study period (1998 – 2011) and the spatial grid consisted of 278 cells each measuring 50 × 50 km. The large scale spatio-temporal model element therefore consisted of 182 924 random variables (47 size class × 14 years × 278 grid cells), which were assumed to follow a log Gaussian distribution that determined the mean of the catch (in numbers).

The second main element in the model, which reflected local patchiness and fish' tendency to aggregate with similar sized individuals on a local scale was the "nugget effect" ($\eta_0(s, j)$). It is a well-known phenomenon that catches of certain fish sizes tend to be overrepresented in trawl hauls compared to the size distribution in the sampled population in the sea, likely due to the size-structured nature of schools or shoals (Kristensen et al., 2013). This local effect was accounted for by modelling the remaining variation among the hauls (within cells) with a Gaussian-distributed mean-zero term of variance σ_N^2 and decorrelation range (*L*) across sizes.

The third main element of the model was the stochastic population dynamics size spectrum ($\phi(s,t)$). It was governed by the McKendrick-von Foerster equation ($\frac{\partial \phi}{\partial t} = -g\frac{\partial \phi}{\partial s} - z$) (Kot, 2001) with an added noise term (ε) applied in every time step to make this model much more flexible than the deterministic counterpart (Kristensen et al., 2013). The constant growth and mortality rates should therefore be interpreted as averages rates over time. The population dynamics were discretized into 47 size classes and 32 time steps per year. Consequently, this was represented by 21 056 random effects (47 size class × 14 years × 32 time steps).

Finally the catch was affected by the catchability of the gear (*sel(s)*) and this effect was implemented as:

$$sel(s) = (1 + 3^{-(2/SR)*(s-\ell_{50}^{Gisund})})^{-1},$$

where *sel(s)* was the selection factor, *SR* was the selection range and ℓ_{50}^{Gisund} was the fish length (*s*) in cm at half selection for the Gisund gear.

The parameters in the model were estimated using the maximum likelihood principle based on the Laplace approximation and thus the estimation follows the principles of Kristensen et al. (2013).

The fitted model was then used to calculate annual estimates of the abundance index of hake in each size class in each 50 x 50 km cell. These spatio-temporal distribution patterns were also transformed into a coastline-oriented coordinate system, to reveal any along-shore migration patterns. This was done by projecting the estimated abundances in the Cartesian coordinate system onto an axis that followed the coastline as a straight line from the Namibia-Angola border (11°E , 17°S) in the North, via Cape Point (18.5°E, 34°S) to east of Port Elizabeth on the South-African south coast (27.5°E, 34°S) (see Fig. 1). Multiannual average distributions were calculated as the unweighted average distribution of multiple years.

For explanatory purposes, the length-based model outputs were presented by both length and absolute age. The length-to-age conversions were done by using the age readings by DAFF (D. Durholtz, DAFF, unpublished data). This was done by calculating the average age by length from the Von Bertalanffy equations fitted to age readings of male and female *M. capensis*, respectively (plot provided in results section). Maps and bar plots were constructed to show mean distributions of *M. capensis* of length groups corresponding (+/- 1.5 cm) to the ages in one year steps from 0.5, the mean size and age when a new cohort first appears in the surveys, to 9.5 years.

Depth data were downloaded as gridded (0.07° lat x 0.07° lon) averages from the NOAA ETOPO1 database (Amante and Eakins, 2009) using the “marmap” package (Pante et al., 2015). Mean depth was calculated for each cell and isobaths were produced for the maps. Finally, abundance in cells with a mean depth exceeding the deepest trawl haul (960 m) was set to 0. The deepest observed *M. paradoxus* catch was at 934 m.

3. Results

The parameter estimates (and associated standard errors) of the model fitted to the catch data are given in Table 1.

Hake densities were found to be correlated in space and size with a spatial de-correlation distance (*H*) of 481 km and a length de-correlation difference (*L*) of 79 cm. These patterns were found to be very stable from year to year with a temporal de-correlation period (*T*) spanning 30.1 years (CV = 7 %) and could therefore be examined as averages over the entire time series.

Estimated variance parameters revealed a roughly equal contribution from spatial large-scale patterns (σ^2 = 20.9) and the nugget effect (σ_N^2 = 12.4). In comparison, the contribution from population dynamics was much smaller (σ_ε^2 = 0.03). The variance in abundance of a given size class at a single point in time and space was therefore completely dominated by large scale spatial effects and local effects rather than demographic effects.

The total mortality rate of *M. paradoxus* was estimated to 0.33 year^{-1} (CV = 67 %). However, this varied through life and between areas. The mortality increased substantially when the fish exceeded approximately 55 cm (Figure 3). The growth rate was estimated to be 8.3 cm year^{-1} (CV = <0.001 %). Despite the very weak population effect, these estimates (mortality and growth) resembled previously reported rates (Figure 3 and 4). However, the cohort signals were too weak to be used for tracking of single cohorts and their effects on spatio-temporal distribution fields were negligible.

M. capensis was not fully recruited to the trawl survey in their first year (Figure 3). This was evident from the estimated selection of the reference gear "Gisund" (ℓ_{50}^{Gisund} = 8.4 cm, SR^{Gisund} = 1.4 cm) and the increase in abundance from 0.3 to 1.3 years (Figure 3).

3.1 Spatial patterns (distribution, migration, population structure)

The spatial distribution of the catch rate of *M. paradoxus* was estimated and illustrated to infer age and size-related migration patterns. This was done for length groups corresponding to the ages from 0.3, the approximate age when a new cohort first appears in the surveys, to 9.3 years.

To examine the alongshore migration patterns, we projected the length-age-specific spatial distributions onto an axis consisting of two straight lines, one from the Namibia-Angola border

(Kunene River mouth) in the North, via Cape Point to Port Elizabeth in the south-east. The alongshore projections (Figure 5 and 6) and distribution maps (Figure 7 and 8) indicated horizontal movements throughout the life span of *M. paradoxus*. The initial distributions of the approximately 0.3- year-olds (recruits) and the 1.3-years olds (juveniles) indicated one main nursery area (Figure 6 and 7). During the first 7 years of the life of *M. paradoxus*, the distribution shifted gradually from year to year, indicating considerable alongshore migrations. In the north, considerable quantities of *M. paradoxus* appeared to move northwards from the area around Orange River - their most likely origin. In lesser number, *M. paradoxus* moved eastwards along the south coast of South Africa. *M. paradoxus* were most widespread at the age of approximately 4.3 years (51 cm) where almost 100 % were mature (50 % mature at 42 cm (Singh et al., 2011)). Later, the distributions progressively contracted in the vicinity of the nursery area (Figure 5, 6 and 8). The movements north of Orange River (the border between Namibia and South Africa) and east of Agulhas thus indicated natal homing as the most parsimonious explanation. Consequently, transboundary movements most likely occurred.

M. paradoxus appeared initially to move to shallower waters at around 80 m depth, after which they gradually moved deeper from approximately 0.5 to 5 years of age. From the age of 5 they were found from 150 to 935 m, but mainly between 350 and 650 m, while moving into slightly shallower waters (Figure 9).

4. Discussion

The present analysis was based on the hitherto largest database of *M. paradoxus* survey data, for the first time including surveys from both the Namibian, Norwegian and South African fisheries research institutes. The quantitative geostatistical modelling exposed spatial migration patterns largely in line with Strømme et al. (2016) that were based on visual inspection of presence/absence outline maps based. Like Strømme et al. (2016) and Le Clus et al. (2005) we assumed that the spatial shifts in distribution over the life span of post-larval *M. paradoxus* were primarily reflecting migration and to a lesser extent mortality, however, the effects of spatial variation in mortality remains to be studied.

4.1 Spatial patterns (distribution, migration, population structure)

The results indicated one primary recruitment/nursery area on the west coast of South Africa and a secondary low-production area around Port Elizabeth on the South Coast. Juveniles initially migrated away from the main recruitment area, followed by natal homing by larger individuals. This pattern was highly consistent through the studies time series as indicated by the very long decorrelation time.

The return migration from Namibia appeared to take place when the hakes exceeded 50 cm. At this size almost 100 % would be mature if they matured at the same size as in South Africa Singh et al (2011), which is in contrast to the very few findings of spawning *M. paradoxus* in Namibian waters (Jansen et al., 2015a). Size of maturation therefore needs to be estimated for the part of the stock that migrates into Namibian waters.

At the South coast of South Africa *M. paradoxus* appeared to move slightly westwards and then stay after reaching the size of maturation. This corresponds to the spawning reported in this area by Jansen et al. (2015a). However, very few recruits were observed, indicating that either they were outside the surveys area, transported by the currents to the west coast before they were caught in the survey, underestimated (unaccounted gear avoidance due to factors such as vertical distribution or gear), or the reproduction in this area was less successful than on the west coast.

The spatial life history patterns thus conform to the concept of one main population unit (stock), but points to an additional smaller component on the eastern part of South Africa's south coast. The level of interconnection (mixing/straying) between these components (stocks) is presently unknown, but appears to exceed the threshold where genetic differentiation occurs in the mitochondrial DNA (Henriques et al., 2016). Furthermore, the rarity of small juveniles in the eastern survey catches is puzzling and calls for field work using other techniques than the standard survey.

M. paradoxus reached its deepest distribution at around 50-55 cm length (Figure 9), where it was abundant at depths deeper that 600 m. These depths were not completely covered by the surveys. This corresponds to an increased mortality at the same sizes (Figure 3), which could be explained by fish moving out of the survey coverage.

4.2 Population dynamics and nugget effects

The effect of the population dynamics in the model was minuscule, this could be a consequence of the year-round spawning and recruitment of *M. paradoxus* combined with the difference in timing of the South African South coast and West coast surveys. Despite this, growth and mortality rates appeared to be relatively well estimated as indicated by the low standard deviations of the estimates and the comparison with values reported from age readings and stock assessments. A plausible explanation for this result, which is consistent with what was found for *M. capensis* (Jansen et al., 2016), is that the variability in the size-structured spatial patterns is so relatively large, that the contribution from the population dynamics is not required to explain patterns in data.

The data and model fit for *M. paradoxus* did not indicate any large spatial differences in small scale variability (nugget effect) that complicated the interpretation of the model fit like for *M. capensis* (Jansen et al., 2016). This is evident from supplementary information 2 that is made for comparison with figure 5 and 6 in Jansen et al. (2016).

To be added: 1. Discuss gear effects. 2. Test sensitivity to the gear effect estimates. How much would the results change if the gear effects changed (Supplementary information 3).

4.2 Model performance and future developments

The GeoPop model has been made possible by Template Model Builder's computational approach to general statistical problems with many unobserved random variables, as well as the availability of memory and processing power through cloud computing. GeoPop represents a major improvement of earlier approaches, specifically by including both population dynamics, large-scale spatial patterns, and small-scale size-structured clustering. Since GeoPop lies at the boundary of what is currently computationally feasible, a number of compromises had to be made with respect to the ecological fidelity of the model, and it is foreseeable that future developments in algorithms and computational resources will allow further refinement of the model assumptions. Here, we list three candidates for such refinements:

1. Currently, the correlation structure in the spatial fields is assumed to be isotropic, i.e. independent of direction. It is plausible that correlations between different locations depend not only on distance, but also on differences in depth or other key habitat parameters. Some extensions are relatively straightforward and could for example be achieved by changing coordinates from latitude and longitude to alongshore distance and depth. However, this solution would have other flaws, as it would e.g. regard an off-shore bank as an extension of the near-coast space. A more general and robust structure could be obtained by modelling the fluxes in space that drive the redistribution of the stock between time points; this could include diffusive fluxes which would be anisotropic, as well as advective fluxes which indicate preferred migrations. While such an extension is appealing from the point of view of first principles in spatial ecology, by explicitly modelling migrations, it would lead to correlation structures that make computations much more demanding. In general, inference in spatiotemporal dynamics, including model selection, is a computationally intensive task in which the trade-off between fidelity and feasibility must constantly be reassessed as computational abilities expand.

2. The growth dynamics and the mortality patterns are grossly simplified, in that both are assumed constant. A major effort would be required to allow changes in growth rates, explained by current size and possibly also environmental covariates, as well as varying mortality, most importantly described by spatiotemporal patterns in fishing effort. Ultimately, the inclusion of such patterns could lead to a spatiotemporal size-based assessment model. The effort required for this development would be very substantial, but single steps in this direction could be pursued.

3. It could be envisioned to include different stock components, differing in timing and location of spawning. This would facilitate the tracking of individual cohorts.

5. Conclusion

The perception of the migration and population patterns derived from the first geostatistical modelling of data from all surveys in the region corresponds largely to the hypothesis and data

plots presented by Le Clus et al. (2005) and Strømme et al. (2016), but differ from the current assessment practices in Namibia and South Africa, where two stocks are assumed to be separated by the national border.

Acknowledgements

We wish to thank the lab and field assistants from MFMR (Namibia), DAFF (South Africa), IMR (Norway) as well as captains and crew of the RV *Africana* and RV *Dr Fridjof Nansen* that sampled and measured hakes analyzed in the present study. The sampling was funded by MFMR (Namibia), DAFF (South Africa) and EAF/Nansen (FAO/Norway). Data analysis and publishing was funded by EuropeAid through the EcoFish project (CRIS Number C-222387).

References

Agenbag, J.J., Shannon, L.V., 1988. A suggested physical explanation for the existence of a biological boundary at 24 30′ S in the Benguela system. South African J. Mar. Sci. 6, 119–132.

Amante, C., Eakins, B.W., 2009. ETOPO1 1 Arc-Minute Global Relief Model: Procedures, Data Sources and Analysis. NOAA Tech. Memo. NESDIS NGDC-24 1–19.

Axelsen, B.E., Johnsen, E., 2015. An evaluation of the bottom trawl surveys in the Benguela Current Large Marine Ecosystem. Fish. Oceanogr. 24, 74–87.

Bloomer, P., Santos, S., Oosthuizen, C., Hoareau, T., Klopper, A., 2009. Hake population genetics: development of microsatellite markers and screening of microsatellite locus variation in Cape hakes, Merluccius paradoxus and M. capensis, from the Namibian and South African coasts. BENEFIT Report, Univ. Pretoria, South Africa.

Botha, L., 1980. The biology of the Cape hake Merluccius capensis Cast. and M. paradoxus Franca. PhD thesis, Stellenbosch Univ. South Africa.

Burmeister, L., 2005. Is there a single stock of Merluccius paradoxus in the Benguela ecosystem? African J. Mar. Sci. 27, 23–32. doi:10.2989/18142320509504065

Burmeister, L., 2001. Depth-stratified density estimates and distribution of the Cape hake Merluccius capensis and M. paradoxus off Namibia, deduced from survey data, 1990–1999. S. Afr. J. Mar. Sci. 23, 347–356.

Fournier, D.A., Skaug, H.J., Ancheta, J., Ianelli, J., Magnusson, A., Maunder, M.N., Nielsen, A., Sibert, J., 2012. AD Model Builder: using automatic differentiation for statistical inference of highly parameterized complex nonlinear models. Optim. Methods Softw. 27, 233–249.

Gordoa, A., Duarte, C.M., 1991. Size-dependent spatial distribution of hake (Merluccius capensis and Merluccius paradoxus) in Namibian waters. Can J Fish Aquat Sci 48, 2095–2099.

Grant, W.S., Becker, I.I., Lesliet, R.W., 1988. Evolutionary divergence between sympatric species of southern African hake, Merluccius capensis. Heredity (Edinb). 61, 13–20.

Grant, W.S., Leslie, R.W., Becker, I.I., 1987. Genetic stock structure of the southern African hakes Merluccius capensis and M. paradoxus. Mar. Ecol. Prog. Ser. 41, 9–20.

Henriques, R., von der Heyden, S., Lipinski, M.R., du Toit, N., Kainge, P., Bloomer, P., Matthee, C.A., 2016. Spatio-temporal genetic structure and the effects of long-term fishing in two partially sympatric offshore demersal fishes. Mol. Ecol. doi:10.1111/mec.13890

Jansen, T., Kainge, P., Singh, L., Strömme, T., Durholtz, M.D., Kathena, J., Wilhelm, M.R., Erasmus, V., Beyer, J.E., 2015a. Spawning Patterns of Shallow-Water Hake (Merluccius capensis) and Deep-Water hake (M. paradoxus) in the Benguela Current Large Marine Ecosystem Shown by Gonadosomatic Index (GSI). Fish. Res. 172, 168–180. doi:10.1016/j.fishres.2015.07.009

Jansen, T., Kristensen, K., Kainge, P., Durholtz, D., Strømme, T., Thygesen, U.H., Wilhelm, M.R., Kathena, J., Fairweather, T.P., Paulus, S., Degel, H., Lipinski, M.R., Beyer, J.E., 2016. Migration, distribution and population (stock) structure of shallow-water hake (Merluccius capensis) in the Benguela Current Large Marine Ecosystem inferred using a geostatistical population model. Fish. Res. 179, 156–167. doi:10.1016/j.fishres.2016.02.026

Jansen, T., Kristensen, K., Payne, M., Edwards, M., Schrum, C., Pitois, S., 2012. Long-term Retrospective Analysis of Mackerel Spawning in the North Sea: A New Time Series and Modeling Approach to CPR Data. PLoS One 7(6), 1–10. doi:10.1371/journal.pone.0038758

Jansen, T., Kristensen, K., van der Kooij, J., Post, S., Campbell, A., Utne, K.R., Carrera, P., Jacobsen, J.A., Gudmundsdottir, A., Roel, B.A., Hatfield, E.M.C., 2015b. Nursery areas and recruitment variation of North East Atlantic mackerel (Scomber scombrus). ICES J.Mar.Sci. 72(6), 1779–1789. doi:10.1093/icesjms/fsu186

Jansen, T., Kristensen, K., van der Kooij, J., Post, S., Campbell, A., Utne, K.R., Carrera, P., Jacobsen, J.A., Gudmundsdottir, A., Roel, B.A., Hatfield, E.M.C., 2014. Nursery areas and recruitment variation of Northeast Atlantic mackerel (Scomber scombrus). ICES J. Mar. Sci. doi: 10.10, 11 pp. doi:10.1093/icesjms/fsu186

Kot, M., 2001. Elements of Mathematical EcologyCambridge University Press. New York.

Kristensen, K., Nielsen, A., Berg, C.W., Skaug, H., Bell, B., 2015. TMB: Automatic Differentiation and Laplace Approximation. J. Stat. Softw. http://arx, 1–21.

Kristensen, K., Thygesen, U.H., Andersen, K.H., Beyer, J.E., 2014. Estimating spatio-temporal

445 dynamics of size-structured populations 336, 326–336.
446 Kristensen, K., Thygesen, U.H., Andersen, K.H., Beyer, J.E., 2013. Estimating spatial-temporal
447 dynamics of size-structured populations. Can J Fish Aquat Sci 99, 1–44.
448 Le Clus, F., Hennig, H..-K.O., Osborne, R.F., Leslie, R.W., 2005. Size-dependent spatial
449 dynamics of deep-water Cape hake Merluccius paradoxus density distribution on two
450 coasts, 1990-2003. Mar. Coast. Manag. South Africa, Demersal Work. Gr. Doc.
451 WG/02/05/D.
452 Lett, C., Veitch, J., van der Lingen, C.D., Hutchings, L., 2007. Assessment of an environmental
453 barrier to transport of ichthyoplankton from the southern to the northern Benguela
454 ecosystems. Mar. Ecol. Prog. Ser. 347, 247–259. doi:10.3354/meps06982
455 Lewy, P., Kristensen, K., 2009. Modelling the distribution of fish accounting for spatial
456 correlation and overdispersion. Can. J. Fish. Aquat. Sci. 66, 1809–1820.
457 Mas-Riera, J., 1991. Changes during growth in the retinal structure of three hake species,
458 Merluccius spp.(Teleostei: Gadiformes), in relation to their depth distribution and feeding. J
459 Exp Mar Biol Ecol 152, 91–104.
460 Nielsen, J.R., Kristensen, K., Lewy, P., Bastardie, F., 2014. A Statistical Model for Estimation of
461 Fish Density Including Correlation in Size, Space, Time and between Species from
462 Research Survey Data. PLoS One 9(6). doi:10.1371/journal.pone.0099151
463 Pante, E., Simon-Bouhet, B., Irisson, J.-O., 2015. marmap: Import, Plot and Analyze
464 Bathymetric and Topographic Data. R package version 0.9.2. http://CRAN.R-
465 project.org/package=marmap.
466 Payne, A.I.L., 1995. Cape hakes. Ocean. life off South. Africa. Ed. by A.I.L. Payne, R.J.M.
467 Crawford. Vlaeb. Publ. Cape Town, South Africa 136–147.
468 Payne, A.I.L., Punt, A.E., 1995. Biology and fisheries of South African hakes (M. capensis and
469 M. paradoxus). Hake Fish. Ecol. Mark. pp. 15–47. Ed. by J. Alheit, T.J. Pitcher. Chapman
470 Hall, London.
471 Rae, C.M.D., 2005. A demonstration of the hydrographic partition of the Benguela upwelling
472 ecosystem at 26° 40’S. African J. Mar. Sci. 27, 617–628.
473 Singh, L., Yolanda, M., Glazer, J., 2011. Merluccius capensis and M. paradoxus length at 50%
474 maturity based on histological analyses of gonads from surveys. DAFF Work. Gr. Doc.

Fish.

Strømme, T., Lipinski, M.R., Kainge, P., 2016. Life cycle of hake and likely management implications. Rev. Fish. Biol. Fish. 26, 235–248. doi:10.1007/s11160-015-9415-9

von der Heyden, S., Lipinski, M.R., Matthee, C.A., 2010. Remarkably low mtDNA control region diversity in an abundant demersal fish. Mol. Phylogenet. Evol. 55, 1183–1188.

Wieland, K., Durholtz, M.D., Fairweather, T., 2013. Environmental effects on hake catchability in the South African West Coast survey. MARAM IWS/DEC13/Ecofish/P3 1–29.

Table 1. Model parameter estimates and standard errors. Parameters with unit "1" are dimensionless.

Symbol	**Description**	**Unit**	**Estimate**	**Standard error**	**CV (%)**
ℓ_{50}^{Gisund}	Fish size at half selection (Gisund)	cm	8.372	0.882	11
SR^{Gisund}	Selection range (Gisund)	cm	1.414	0.308	22
g	Growth rate	cm/year	8.320	<0.001	<0.001
z	Total mortality	1/year	0.325	0.218	67
σ_{ε}^2	Variance of population dynamics	1	0.033	0.006	18
T	Decorrelation time	year	30.088	2.220	7
L	Decorrelation size	cm	79.069	1.894	2
H	Spatial decorrelation distance	km	480.606	31.087	6
σ^2	Variance of the space-time-size correlations	1	20.934	1.265	6
σ_N^2	Variance of the nugget effect	1	12.350	0.283	2

490 **Figures**

491

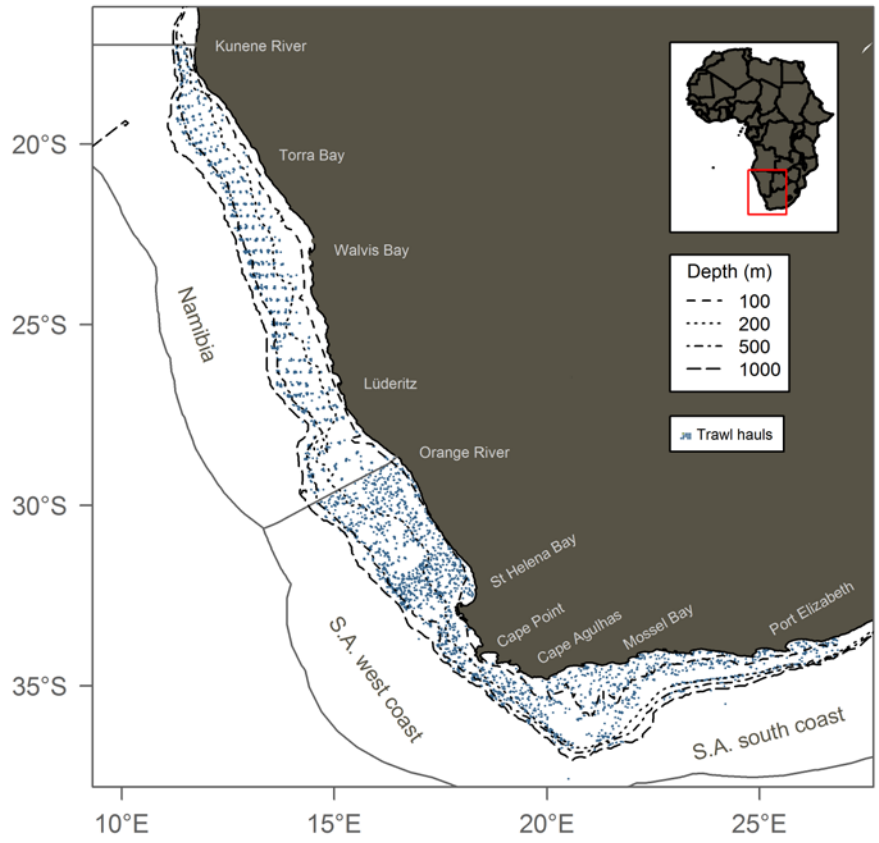

492

493 Figure 1. Map of study area with sample locations (dots), isobaths and place names referred to in
494 the text.

495

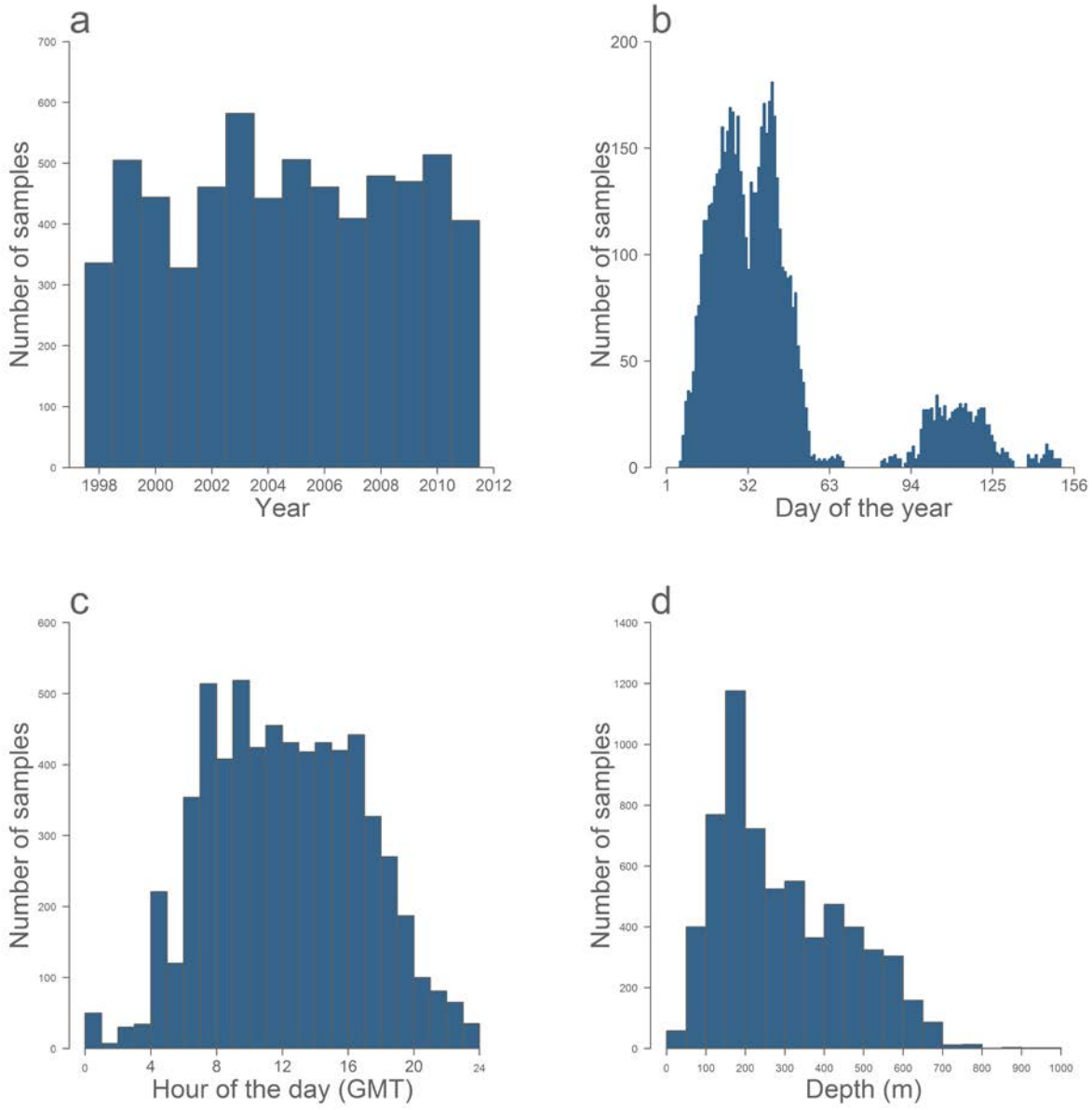

Figure 2. Demersal trawl survey samples (trawl hauls) by year (a), ordinal day (b), hour of the day (c) and depth (d).

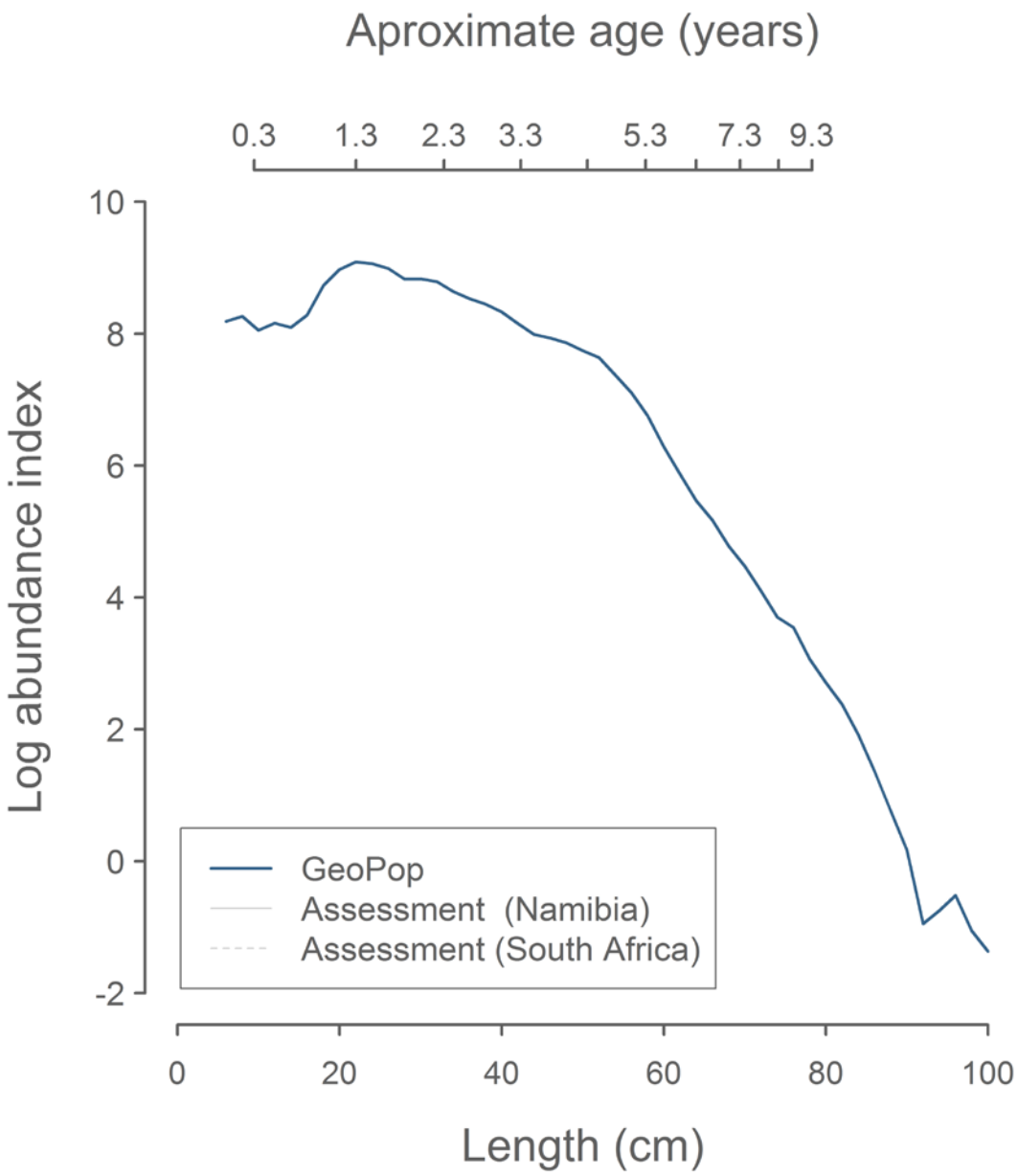

Figure 3. Log abundance index of deep-water hake (*M. paradoxus*) by length and approximate age (blue line). Inclination equals the total mortality. The mortality estimated in the Namibian and South African stock assessments are indicated by grey lines [To be added] (mean Z in South Africa from 1998 to 2012 from Rademeyer (2012) and in Namibia from 1998 to 2011 from Kathena et al. (2015)).

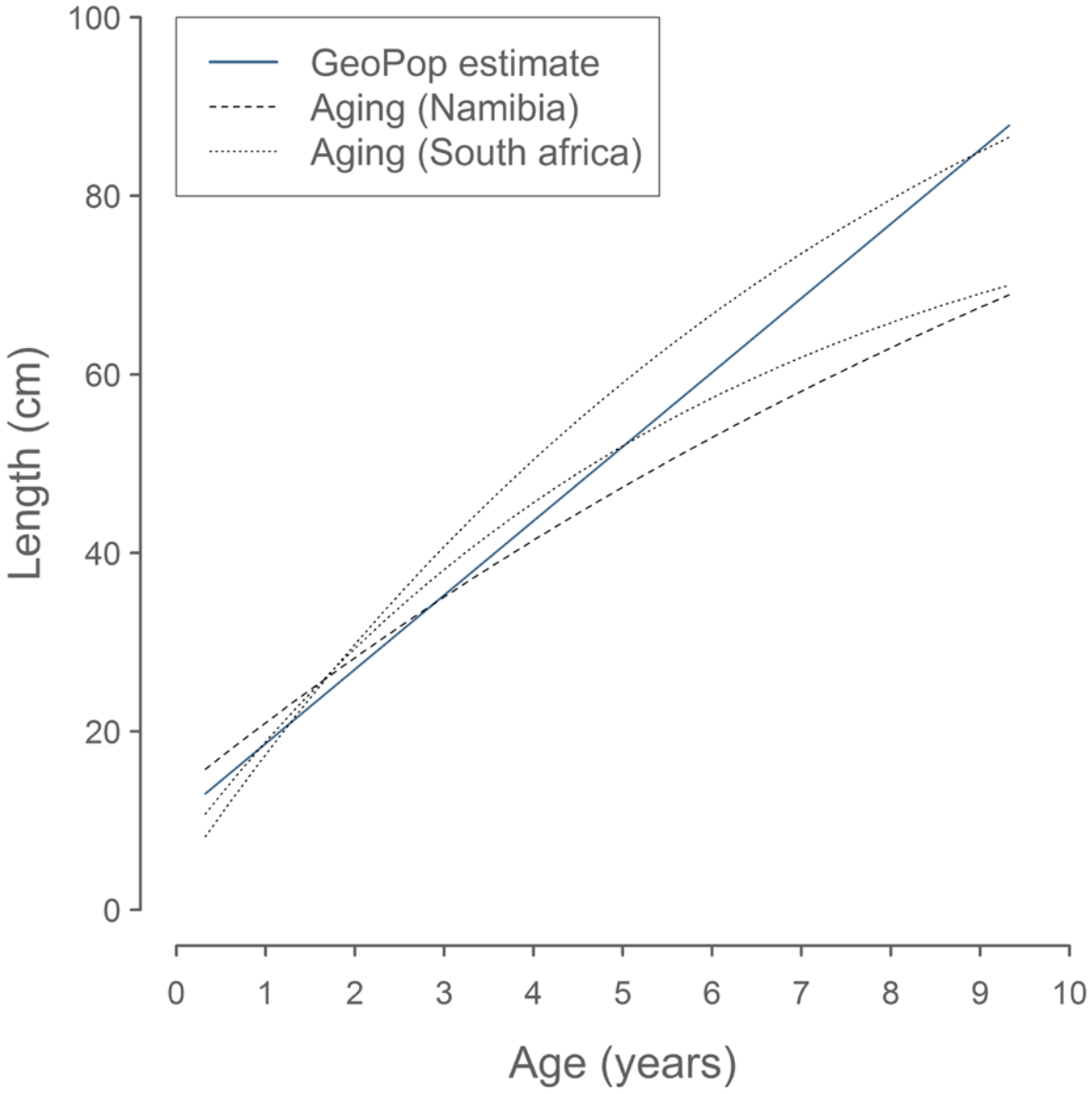

507

508 Figure 4. Comparison of growth rate estimates for deep-water hake (*M. paradoxus*). Estimate
509 from the GeoPop model (*8.4 cm year^{-1}from first surveyed at an age of approximately* 0.3
510 years corresponding to 9.5 cm according to South African age readings, blue straight line),
511 Von Bertalanffy equations fitted to South African age readings (females: upper dotted line;
512 males: lower dotted line), Namibian age reading (dashed line).

513

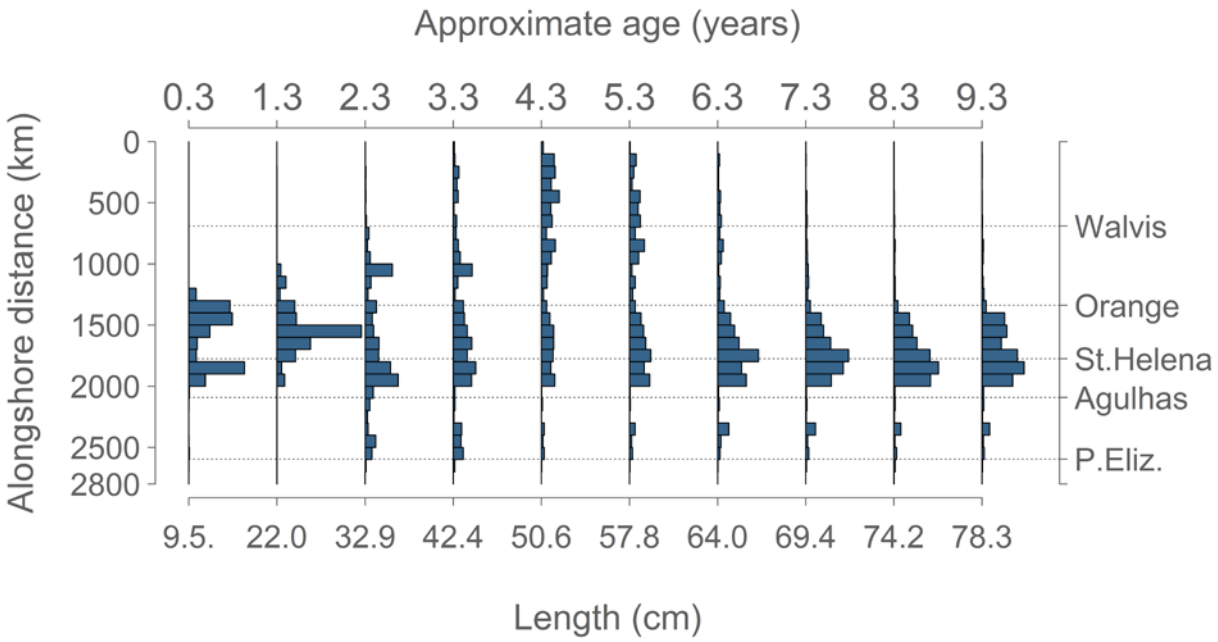

Figure 5. Alongshore distribution of number of deep-water hake (*M. paradoxus*) by length and approximate age estimated by GeoPop model after removal of local noise (nugget effect). The distributions are standardized for each age, so the areas of the bars are the same for all age distributions. The spatial distributions were projected onto a curvilinear axis following the coastline from the Namibia-Angola border (Kunene River) in the North to Port Elizabeth in the south-east.

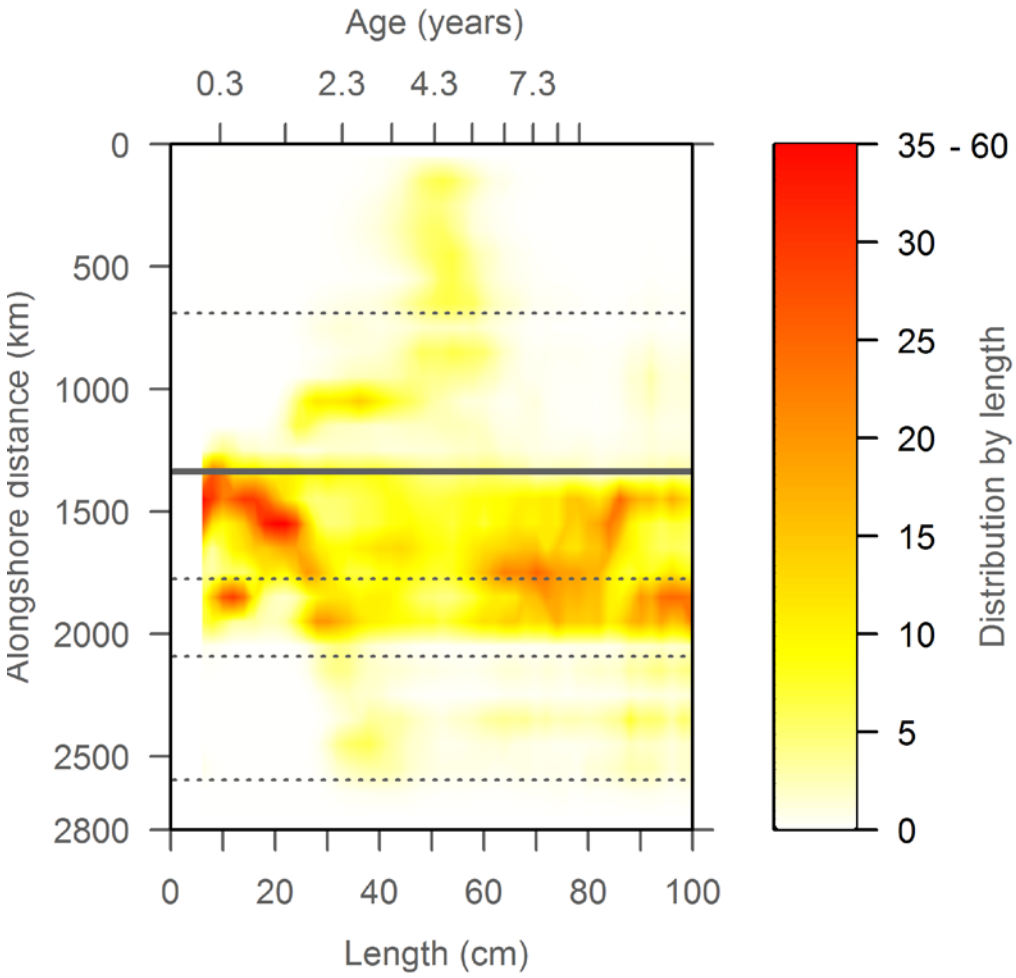

Figure 6. Alongshore distribution of number of deep-water hake (*M. paradoxus*) by length and approximate age estimated by GeoPop model after removal of local noise (nugget effect). The distributions are standardized for each 2-cm length class. The spatial distributions were projected onto a curvilinear axis following the coastline from the Namibia-Angola border (Kunene River) in the North to Port Elizabeth in the south-east.

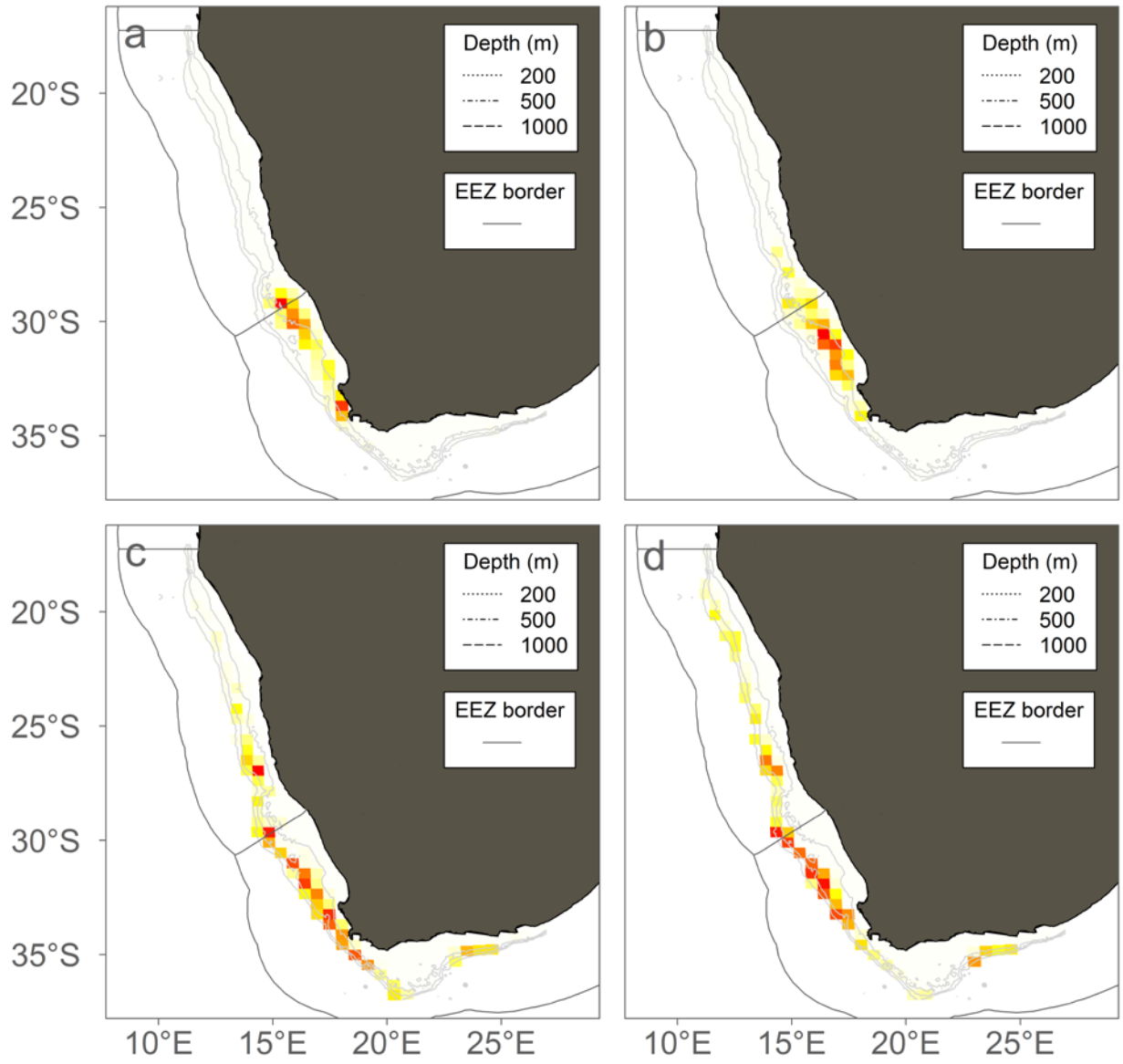

Figure 7. Distribution maps of deep-water hake (*M. paradoxus*) at the age of approximately 0.3 years (a), 1.3 years (b), 2.3 years(c) and 3.3 years (d). The distributions are illustrated as cumulative fractions, e.g. the sum of all areas with the color corresponding to 40 % represents 40 % of the total.

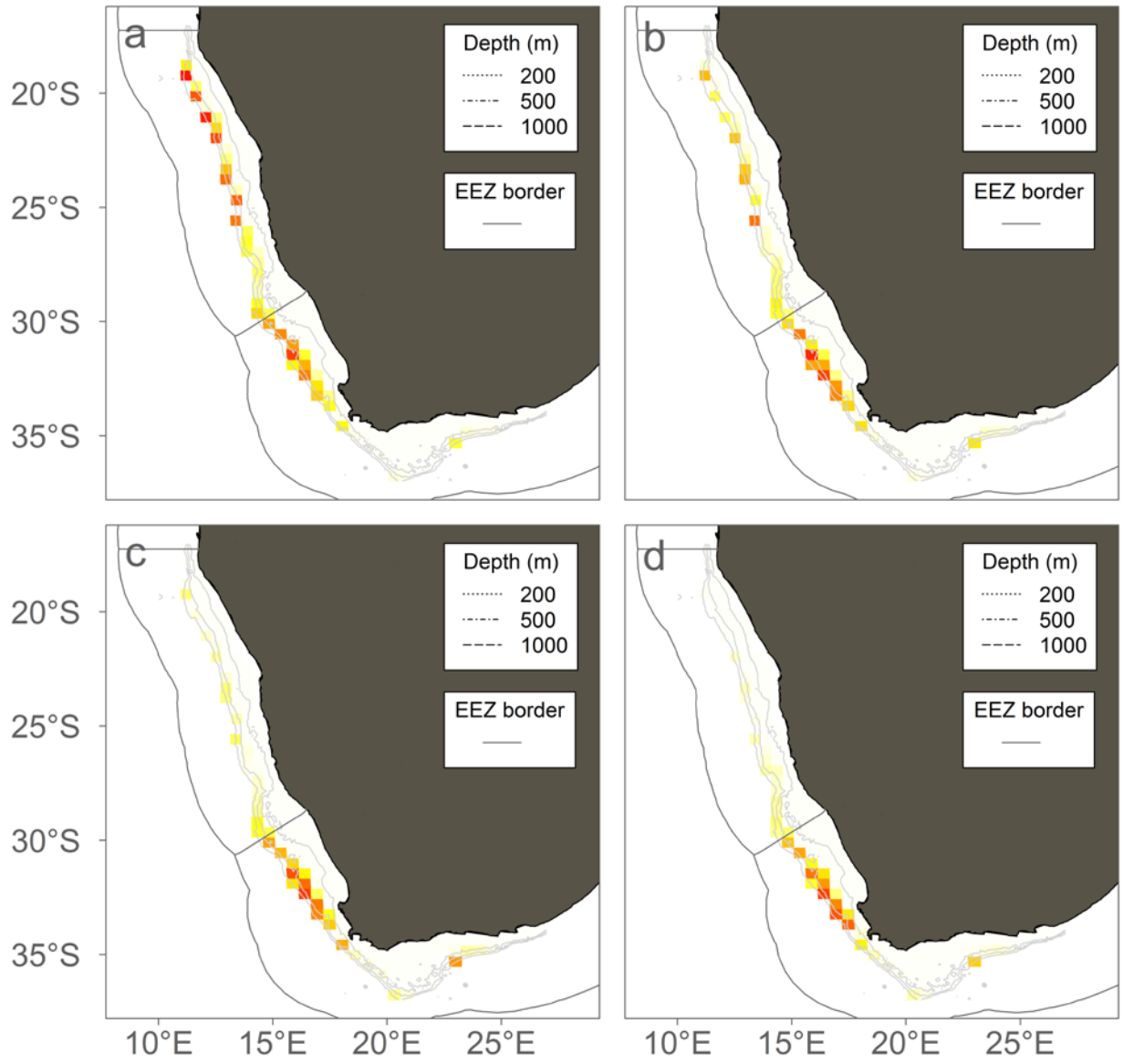

Figure 8. Distribution maps of deep-water hake (*M. paradoxus*) at the age of approximately 4.3 years (a), 5.3 years (b), 6.3 years(c) and 7.3 years (d). The distributions are illustrated as cumulative fractions, e.g. the sum of all areas with the color corresponding to 40 % represents 40 % of the total.

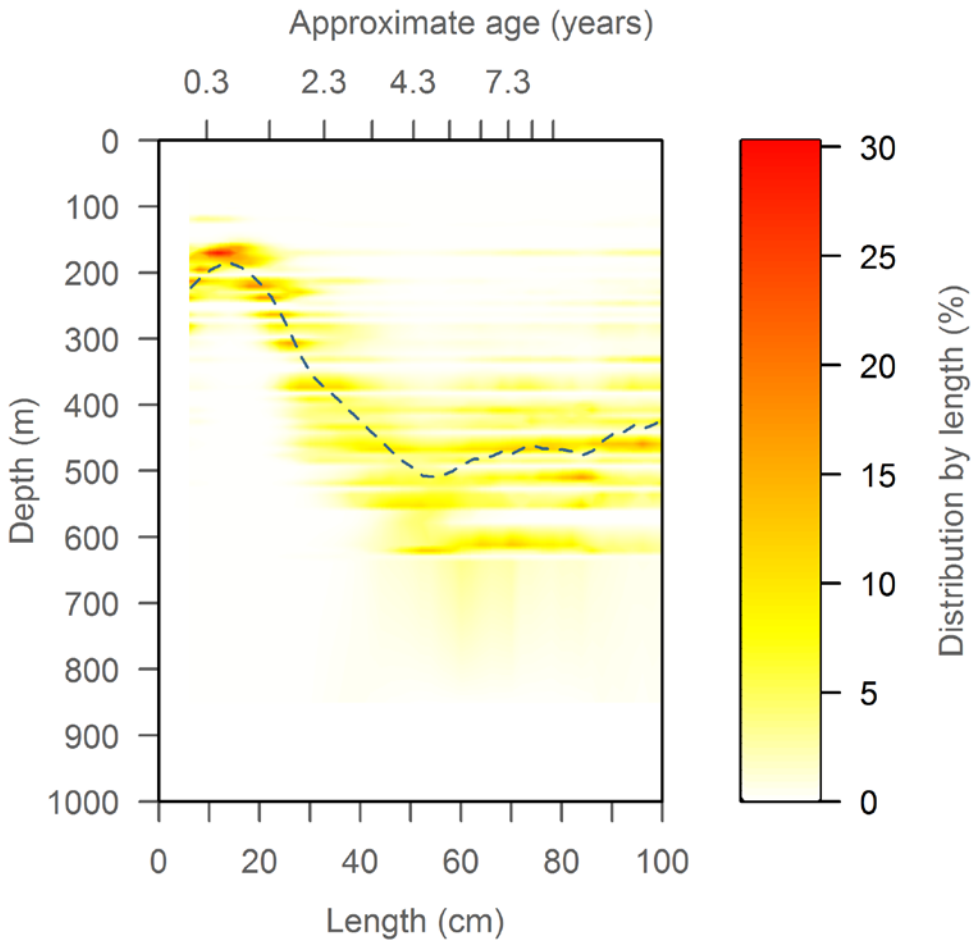

Figure 9. Depth distribution of deep-water hake (*M. paradoxus*) by length and approximate age. Blue dashed lines indicate the weighted mean depth.

Supplementary information

Supplementary information 1. The gear effect on catch rates of *M. paradoxus*.

Supplementary information 2. No large scale spatial bias in nugget effect.

Supplementary information 3. Sensitivity test for the gear effect on the catch rates of *M. paradoxus* [Not done yet].

552

553

554

Suppl. info. 1: The gear effect on catch rates of *M. paradoxus*

As detailed in Materials and Methods, the data base for the present study includes catch rates with different gears. The study must take the difference in the size selectivity and efficiency of the different gears into account, to avoid spurious patterns and bias in the estimated spatial distributions of the stock. Here, we describe how the catches from the R/V Africana are converted to equivalent catches that we can asssume would have been obtained with Gisund. We refer to this as "gear intercalibration".

We constructed a statistical method for intercalibration, i.e. determining the relative selectivity of two gear types, based on data from paired trawl hauls. The model estimates the size spectrum of the underlying population at each station, size-structured clustering of fish at small temporal and spatial scales, in addition to the relative selectivity of the two gears in each length class. The statistical assumption is Poisson distributed catches conditional on log-Gaussian variables that describe the expected catches, which allows for overdispersion and correlation between catch counts in neighboring size classes.

SI 1.1: Statistical model

The intercalibration model is a statistical model which explains the size composition of the catch in survey trawl hauls. The model is a non-linear mixed effect model, in which we do inference using numerical maximum likelihood estimation, employing the Laplace approximation to integrate out random effects.

The observed quantities are count data, N_{ijk}, which represents number of individuals caught at station $i = 1, \ldots, n_s$, with gear $j = 1, 2$, and in length group $k = 1, \ldots, n_l$. Here, the length groups are 2 cm length classes starting at 10 cm.

We assume that these catches are Poisson distributed, conditional on the swept area A_{ij} and three sets of random variables, which all depend on the size class k: First, the local background size spectrum Φ_{ik}, which is specific to the station, second, haul-specific fluctuations R_{ijk} in the size spectrum, and third, the relative selectivity S_{jk} which is specific to the gear. More specifically, Φ_{ik} represents the size composition of the fish at station i, as would be observed with a hypothetical gear with "typical" size selectivity, so that $\exp(\Phi_{ik})$ is the expected number of fish caught in size group k at station i with a hypothetical gear which lies in between the two gears $j = 1$ and $j = 2$.

Next, the haul-specific fluctuations R_{ijk} are akin to the "nugget effect" in spatial statistics, and represents small-scale clustering of fish. This is particular to both stations and gear, since the paired hauls are done at slightly different locations and times, and therefore these clusters have moved or regrouped between hauls at the same station.

Finally, the selectivity S_{jk} is the main object of interest, and represents the selectivity of gear j in size group k. Since we do not know the actual size

distribution of the stock, we cannot estimate the absolute selectivity, but only the relative selectivity between the two gears. This corresponds to enforcing $S_{1k} = -S_{2k}$

Given these random variables Φ, R, S, we assume that count data is Poisson distributed:

$$N_{ijk}|\Phi, R, S \sim \text{Poisson}(A_{ij} \cdot \exp(\Phi_{ik} + S_{jk} + R_{ijk}))$$

The swept area A_{ij} is an input to the model. The unobserved random variables, Φ, R and S, are given prior distributions: The size spectrum at each station, i.e. Φ_{ik}, is considered a random walk over size groups:

$$\Delta\Phi_{ik} \sim N(0, \sigma_\Phi^2) \text{ for } k = 1, \ldots, n_l - n_\Phi \quad .$$

Here, Δ is the difference operator. This enforces continuity in the size spectrum; the most probable spectrum is flat. To ensure that the spectrum is a well defined stochastic process, we complement this with initial conditions

$$\Phi_{ik} \sim N(0, \sigma_1^2) \text{ for } k = 1 \quad .$$

Here, the variance σ_1^2 is fixed at a "large" value 10. In contrast, the parameter σ_Φ^2 is estimated. We assume independence between stations, i.e. we do not attempt to model any large-scale spatiotemporal structure of the population. We note that this is the main difference between this model and the GeoPop model, where emphasis is exactly on this spatiotemporal structure.

The residual or "nugget effect" R_{ijk} models size-structured clustering of the fish at small spacial and temporal scales. Thus, this effect is independent between hauls, even those taken at same station i but with different gear j. For a given haul, i.e. for given station i and gear j, the nugget effect is a mean 0 first order autoregressive process of size, with a variance σ_N^2 and correlation coefficient ϕ which is estimated.

The relative selectivity S_{jk}, which we aim to estimate, is modeled as a random walk in size:

$$\Delta S_{jk} \sim N(0, \sigma_S^2) \text{ for } k = 1, \ldots, n_l - n_S$$

We assume infinite variance on the first size group, S_{j1}, i.e. only the increments in the selectivity process enter into the likelihood function.

	Africana Old		Africana New	
Parameter	Estimate	Std. Error	Estimate	Std. Error
$\log \sigma_\Phi$	0.077	0.02	0.17	0.02
ϕ	0.927	0.01	0.92	0.01
$\log \sigma_N$	-0.039	0.05	-0.08	0.05
$\log \sigma_S$	-3.145	0.25	-2.76	0.24

Table 1: Parameter estimates

SI 1.2: Implementation

The statistical model in the previous defines the joint distribution of the count data, N, and the unobserved random variables Φ, R, S, for given parameters σ_S, σ_Φ, and the two parameters (scale and range) defining the nugget effect. The unobserved Φ, R and S are integrated out using the Laplace approximation, to yield the likelihood function as a function of the four parameters. The likelihood function is maximized to yield estimates of the four parameters, after which the posterior means of the Φ, R, and in particular S are reported.

The computations are performed in `R` version 3.1.2 (R Core Team, 2015); we use the Template Model Builder (TMB) package (Kristensen et al., 2016) for evaluating the likelihood function and its derivatives.

SI 1.3: Data

The data base consisted of a total of 236 pairs of trawl hauls performed by RVs Africana and Dr. Fridtjof Nansen. The Gisund gear was used onboard Fridtjof Nansen, while RVs Africana deployed two gear types: "Africana Old" (108 hauls) and "Africana New" (128 hauls). Catch in numbers per length group and the swept area (hauling distance multiplied by wing spread) were available for each haul.

SI 1.4: Results

The obtained intercalibration curves are seen in figure 1. Notice that Gisund overall is more effective than both the Old and the New Africana, in particular in the small size classes. The difference between size classes is statistically significant ($p < 10^{-4}$). For size classes larger than 30 cm, say, the intercalibration curves show little variation with size and although this has not been tested, it is plausible that these variations are not statistically significant. Estimated parameters are seen in table 1.

References

Kristensen K, Nielsen A, Berg C, Skaug H (2016) TMB: Automatic differentiation and Laplace approximation. *J. Stat. Softw* 70.

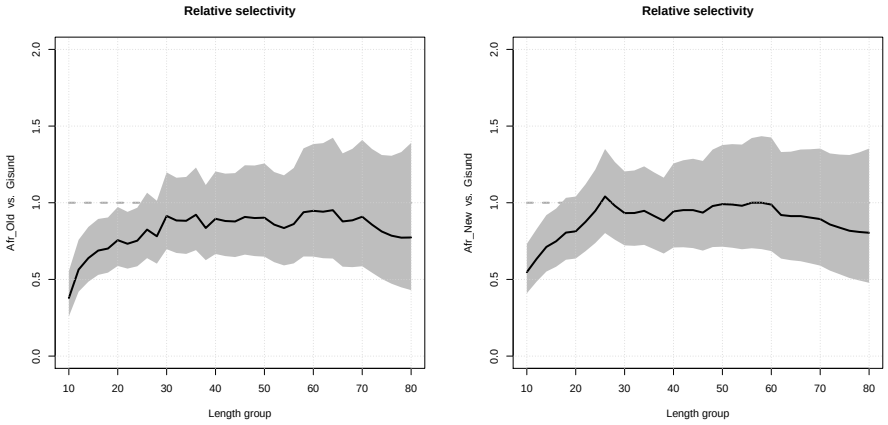

Figure 1: Relative selectivity (gear calibration factor), comparing catches of M. paradoxus with Gisund gear and the "Old" and "New" gear on the R/V Africana. Large values indicate that Africana is more effective. Solid curve: Estimated relative selectivity (posterior mode). Grey region: Marginal 95 % confidence intervals.

R Core Team (2015) *R: A Language and Environment for Statistical Computing* R Foundation for Statistical Computing, Vienna, Austria.

Supplementary information 2

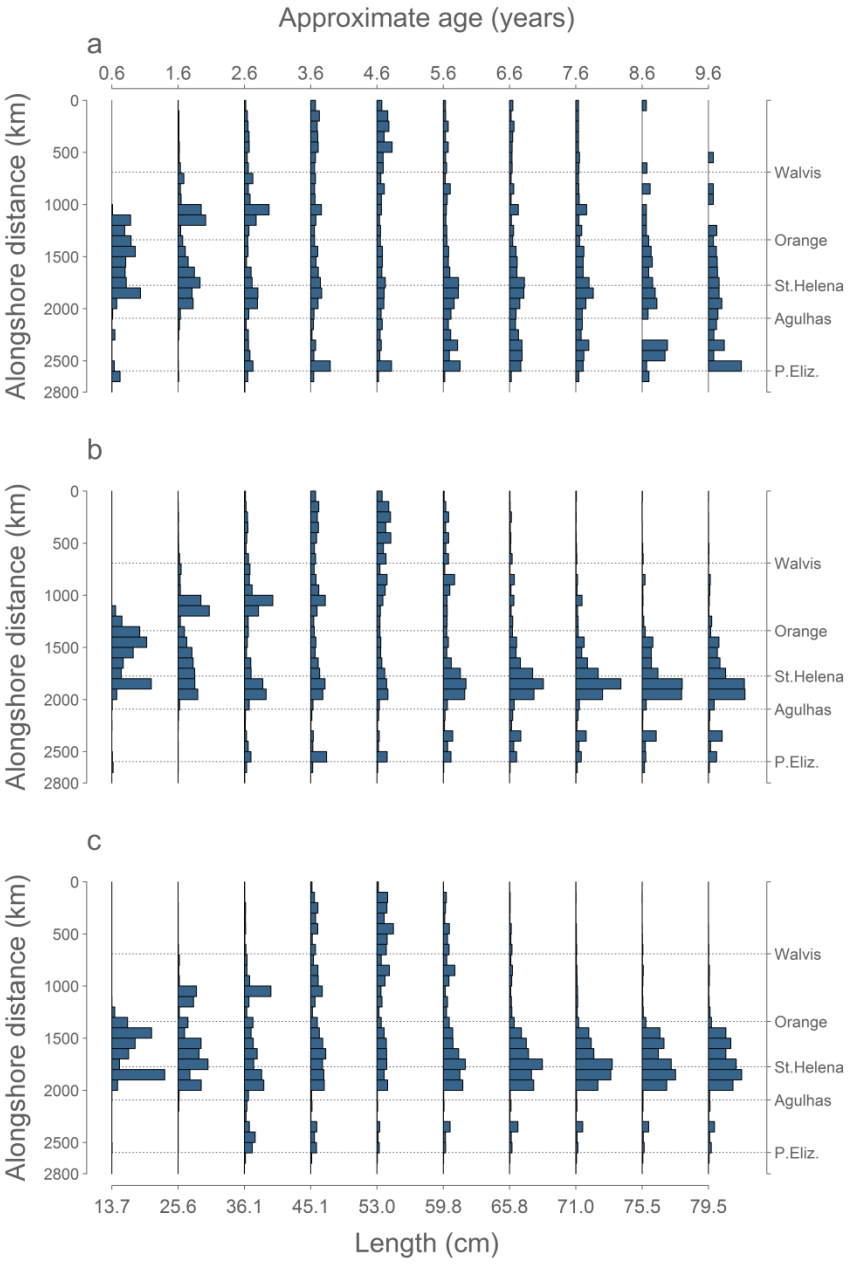

Figure SI2.1. Alongshore distribution of number of deep-water hake (*M. paradoxus*) by size and approximate age. Simple average of catches (a), GeoPop model fit (b) and GeoPop model after removal of local noise (nugget effect) (c). The spatial distributions have been projected onto a curvilinear axis following the coastline from the Namibia-Angola border (Kunene River) in the North to Port Elizabeth in the south-east. This figure is made for comparison with figure 5 in Jansen et al. (2016) and is therefore made in the same design (Jansen et al., 2016).